Analytical investigation of mutual interference between automotive FMCW radar sensors

M. Goppelt[1], H.-L. Blöcher[2] and W. Menzel[1]

[1]Institute of Microwave Techniques, University of Ulm, Germany
[2]Group Research & Advanced Engineering, Daimler AG, Ulm, Germany

***Abstract*— Radar sensors are key components of modern driver assistance systems. Mutual interference was identified as a problem of increased importance because of the appearance of safety functions and the increasing rate of vehicles equipped with radar sensors. This paper describes mutual interference between automotive FMCW radar sensors. Analytical formulas were derived to be able to calculate the probability for ghost targets and the interference power per frequency bin. The results of the analytical calculations are compared with simulation results on the basis of a simple interference scenario with interference from an oncoming vehicle.**

***Index Terms*— Automotive components, Millimeter wave radar, Mutual coupling, Sensor systems, Radiofrequency interference**

I. Introduction

Automotive radar sensors are used for automotive comfort functions and automotive safety functions, e.g. adaptive cruise control (ACC) or collision mitigation systems (CMS). The reception of unwanted signals from other automotive radar sensors is usually called mutual interference between automotive radar sensors [1]–[3]. Such interference can lead to ghost targets or to reduced sensitivity. In the simple mutual interference scenario in Fig. 1 the radar sensor receives direct interference from an oncoming vehicle. Mutual interference was identified as a problem of increased importance because of the appearance of safety functions and the increasing rate of vehicles equipped with radar sensors. In a previous publication by Daimler and the University of Ulm mutual interference between frequency-modulated continuous wave (FMCW) radar sensors and pulsed radar sensors was described qualitatively, and the simple mutual interference scenario in Fig. 1 was analyzed up to the interference power level at the receive antenna port [4]. In the present publication the qualitative description is enhanced by a quantitative analytical calculation of the probability for ghost targets and of the interference power per frequency bin. The simple mutual interference scenario in Fig. 1 is analyzed up to the first signal processing stage of the receiver.

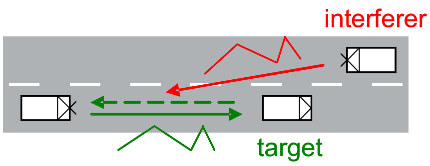

Fig. 1. Simple mutual interference scenario with direct interference from an oncoming vehicle (the interfering radar sensor radiates directly into the own radar sensor).

II. Ghost Targets

For the analysis of the case of FMCW radar sensors interfering with an FMCW radar sensor, the block diagram depicted in Fig. 2 was used including a windowing function (pre block) and a fast Fourier transform (FFT block) as first signal processing stage. For the following analytical calculations the assumption of a linear receiver was made. Both for the analytical calculations and for the simulation interference from an identical FMCW radar sensor with the same start frequency was regarded, as can be seen in the upper diagrams of Figs. 3 and 4. The duration of the short ramps T_2 is only one third of the duration of the long ramps T_1 to be able to resolve the ambiguities in the range-Doppler plane in multi target situations [5]. The interference signal in Fig. 3 creates constant intermediate frequencies (IF) for each ramp of the local oscillator signal (LO signal) which lie in the passband of the anti-aliasing low-pass filter (AA LP block in Fig. 2). These constant frequencies (see lower diagram of Fig. 3) will be interpreted as targets which are usually called ghost targets. The probability p_{ghost} that an interference signal from an identical FMCW radar sensor with the same start frequency creates ghost targets for all ramps is described quantitatively by (1):

$$p_{ghost} = \frac{2 \cdot t_{shift,max}}{T} = \frac{2 \cdot \frac{f_{IF,max}}{S} \cdot T_2}{T} \qquad (1)$$

The underlying assumption is that the time shift t_{shift} of the interference signal is equally distributed between 0 and T. Larger time shifts than the maximum time shift $t_{shift,\,max}$ lead to

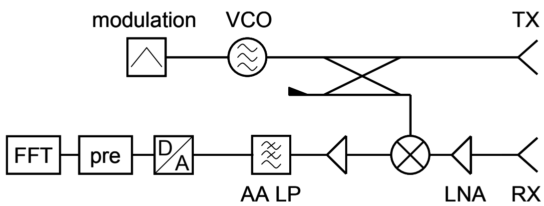

Fig. 2. Block diagram of a simple generic frequency-modulated continuous wave (FMCW) radar for the analysis of the case of FMCW radar sensors interfering with an FMCW radar sensor.

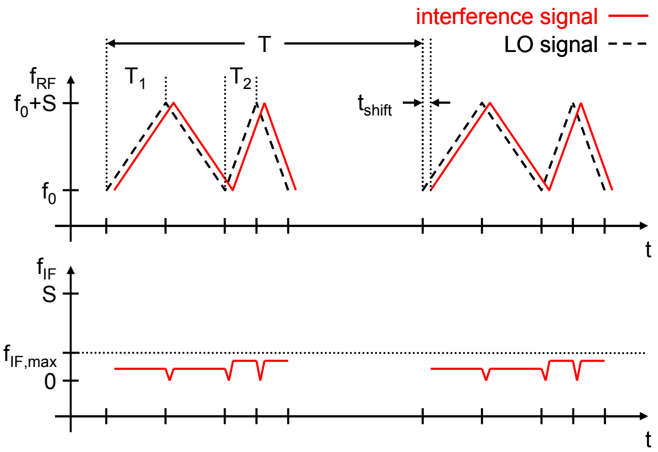

Fig. 3. The upper diagram shows the course of the radio frequency (RF) over time for the local oscillator (LO) signal of the own FMCW radar sensor and for the signal of the interfering FMCW radar sensor. The lower diagram shows the course of the intermediate frequency (IF) over time (at the IF port of the mixer).

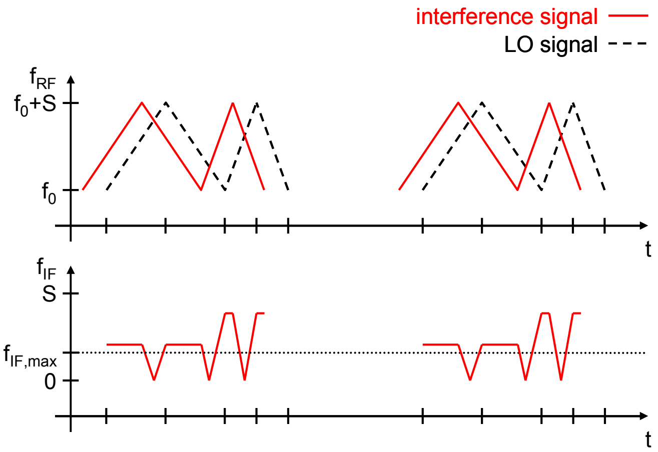

Fig. 4. Like in Fig. 3, the upper diagram shows the course of the RF over time for the LO signal of the own FMCW radar sensor and for the signal of the interfering FMCW radar sensor. The lower diagram shows the course of the IF over time (as in Fig. 3).

higher frequencies than $f_{IF,\,max}$ for the short ramps with the duration T_2, with the result that no ghost targets are created for the short ramps. The calculation of the probability with the parameters chosen for the simulation yielded a value of 125 ppm. The presence of more than one interferer was also regarded. The probability $p_{ghost}(n, N)$ for n interferers out of a total of N interferers to create ghost targets is quantitatively described by (2):

$$p_{ghost}(n, N) = p_{ghost,(1)}^{n} \cdot \left(1 - p_{ghost,(1)}\right)^{N-n} \tag{2}$$

The probability for one or more interferers to create ghost targets during the course of meeting 1000 oncoming interferers amounts to 11.8 percent. For the case of non-identical start frequencies, however, this value can be considerably lower. For the simulation the target power level

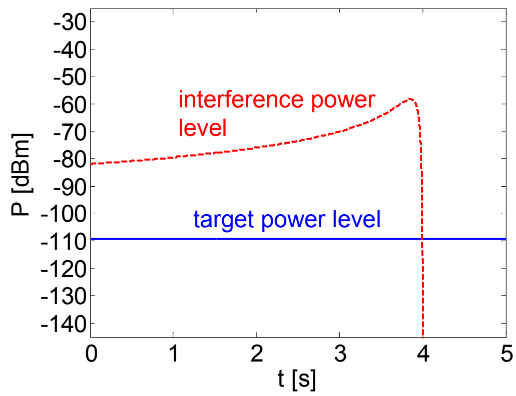

Fig. 5. The analytically calculated power levels for the mutual interference scenario in Fig. 1. The interferer starts at a distance of 120 meters, the vehicles travel at 15 meters per second.

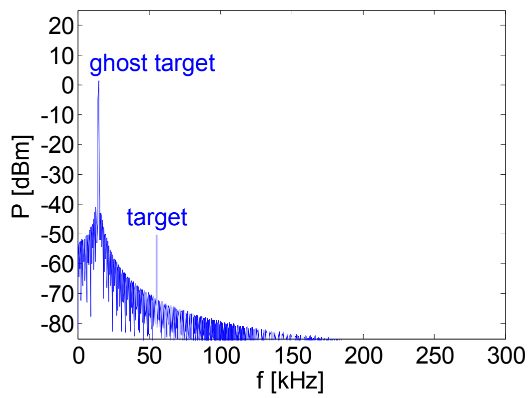

Fig. 6. The power spectrum calculated from the fast Fourier transform (FFT) of the first ramp with the interferer at a distance of 4.5 meters.

and the interference power level for the mutual interference scenario in Fig. 1 were calculated analytically, the result is depicted in Fig. 5. The interferer started at a distance of 120 meters, the snapshot in Fig. 6, which is the power spectrum calculated from the FFT of the first ramp, was taken with the interferer at a distance of 4.5 meters. The interference power level (Fig. 5) at that point was at -58 dBm, 51.1 dB above the target power level, however, still far below the 1 dB compression point of typical mixers for the frequency range of 79 GHz (e.g. -3 dBm). The chosen voltage range of the analog-to-digital converter of 1 V (peak-to-peak voltage) was not exceeded. Whether false targets created by an oncoming interferer can lead to a ghost track could not yet be investigated, tracking has not been included in the simulation model so far.

III. Reduced Sensitivity

The interference signal in Fig. 4 creates constant intermediate frequencies which lie outside of the passband of the anti-aliasing low-pass filter. The falling and rising IF ramps going into the passband and coming out of the passband result in wideband IF signals which can reduce the sensitivity of the radar sensor. The power per frequency bin $P_{\Delta f}$ of the wideband signal generated by an interfering RF ramp is lower than the power level P_{IF} of the constant frequencies in the lower diagram of Fig. 3 by the factor:

$$\frac{P_{IF}}{P_{\Delta f}} = \frac{1}{2} \cdot T_{ramp}^2 \cdot \left| \frac{f_{stop} - f_{start}}{T_{ramp}} - \frac{f_{stop,int} - f_{start,int}}{T_{ramp,int}} \right| \quad (3)$$

Prerequisite for the estimation is that the IF signal generated by the interfering RF ramp sweeps completely through the passband of the anti-aliasing low-pass filter with a falling and a rising IF ramp. The parameters f_{start}, f_{stop} and T_{ramp} are the start frequency, the stop frequency and the ramp duration of the LO ramp, while $f_{start,\,int}$, $f_{stop,\,int}$ and $T_{ramp,\,int}$ refer to the interfering ramp (see Fig. 7). The estimation was derived from the interference power per frequency bin $P_{\Delta f}$ (4), the dwell time per frequency bin (5) and the frequency resolution (6):

$$P_{\Delta f} = \frac{t_{bin}}{T_{ramp}} \cdot P_{IF} \quad (4)$$

$$t_{bin} = 2 \cdot \frac{\Delta f}{\left| \frac{f_{stop} - f_{start}}{T_{ramp}} - \frac{f_{stop,int} - f_{start,int}}{T_{ramp,int}} \right|} \quad (5)$$

$$\Delta f = \frac{1}{T_{ramp}} \quad (6)$$

Since the wideband signal generated by an interfering RF ramp results from the superposition of a falling and a rising IF ramp, the maximum possible power per frequency bin $P_{\Delta f,\,max}$ is twice the calculated power per frequency bin $P_{\Delta f}$ (constructive superposition). The constructive superposition power per frequency bin for more than one interfering RF ramp can be calculated with (7) which performs a summation of the individual constructive superposition amplitudes (N interfering RF ramps):

$$P_{\Delta f,\,max} = \left(\sum_{i=1}^{N} \sqrt{2 \cdot P_{\Delta f,\,i}} \right)^2 \quad (7)$$

The simulation snapshot was again taken with the interferer at a distance of 4.5 meters with the signal constellation as shown in Fig. 8. The maximum possible interference power per frequency bin $P_{\Delta f,\,max}$ was then calculated with (3) and (7) and compared to the power spectrum at the IF port of the mixer (see Fig. 9). It can be seen that $P_{\Delta f,\,max}$ shown as a dashed red line is not exceeded. $P_{\Delta f,\,max}$ is 50.1 dB lower than P_{IF}. The time samples taken by the analog-to-digital converter at the output of the anti-aliasing low-pass filter (shown in

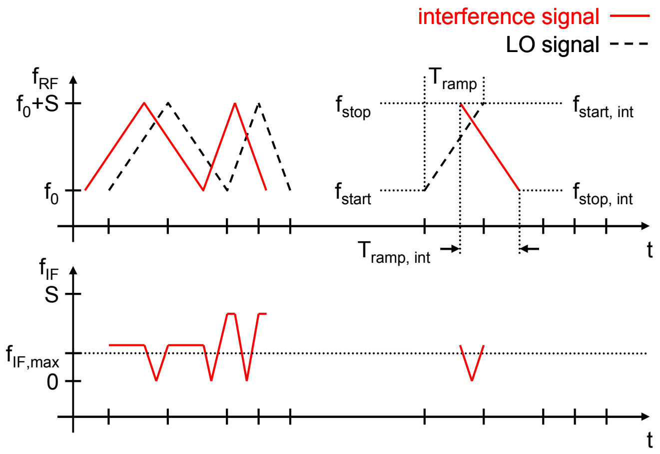

Fig. 7. An illustration of the parameters used in (3).

Fig. 10) are weighted with a Hamming windowing function before the FFT is calculated. The resulting power spectrum calculated from the FFT is depicted in Fig. 11. If the target is detected or not depends in reality on whether the superposition of target signal and interference signal lies above the constant false alarm rate (CFAR) threshold.

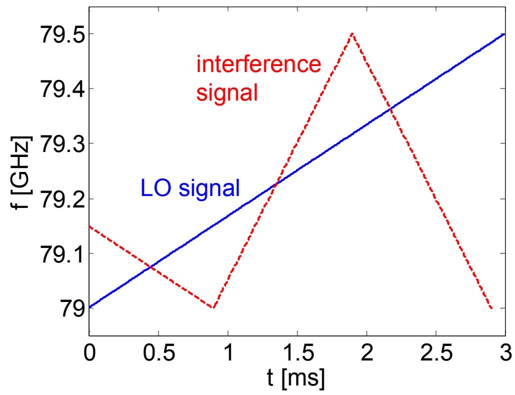

Fig. 8. The course of the local oscillator (LO) frequency of the own FMCW radar sensor over time along with the course of the frequency of the interfering FMCW radar sensor over time.

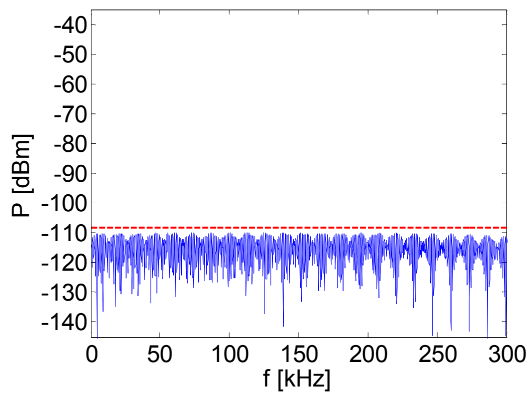

Fig. 9. The power spectrum at the IF port of the mixer, the dashed red line represents the analytically estimated maximum possible interference power per frequency bin.

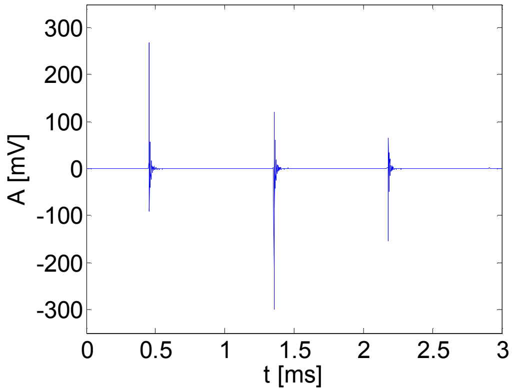

Fig. 10. The time samples taken by the analog-to-digital converter at the output of the anti-aliasing low-pass filter (AA LP block in Fig. 2).

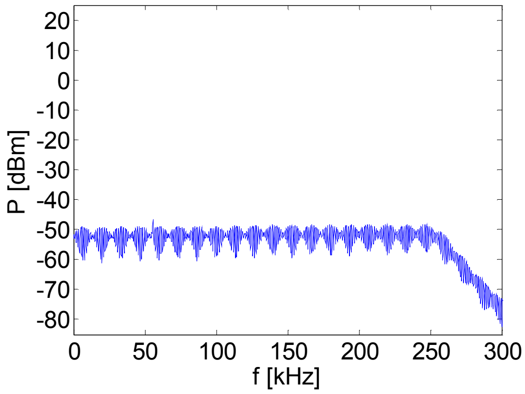

Fig. 11. The power spectrum calculated from the FFT of the first ramp of the LO signal with the interferer at a distance of 4.5 meters.

IV. Conclusion

It was shown how interference between FMCW radars can lead to ghost targets or to reduced sensitivity. Analytical formulas were given for the calculation of the probability for ghost targets and the interference power per frequency bin for the case of one or more FMCW radar sensors interfering with an FMCW radar sensor.

Acknowledgment

The authors wish to thank the German Federal Ministry of Education and Research (BMBF) for funding this work within the “Radar on Chip for Cars” (RoCC) project.

References

[1] Brooker, G.: Mutual Interference of Millimeter-Wave Radar Systems, IEEE Transactions on Electromagnetic Compatibility, 49, 170–181, 2007.

[2] Oprisan, D. and Rohling, H.: Analysis of Mutual Interference between Automotive Radar Systems, International Radar Symposium, Berlin, Germany, 2005.

[3] Tullsson, B.: Topics in FMCW Radar Disturbance Suppression, Radar 97, Edinburgh, United Kingdom, 1997.

[4] M. Goppelt, H.-L. Blöcher and W. Menzel: Automotive radar – investigation of mutual interference mechanisms, Advances in Radio Science, 8, 55–60, 2010.

[5] H. Rohling and M.-M. Meinecke: Waveform Design Principles for Automotive Radar Systems, CIE International Conference on Radar, Beijing, China, October 2001